HAL
open science

Shaping physical properties of galaxy subtypes in the VIPERS survey: Environment matters

M. Siudek, K. Malek, A. Pollo, A. Iovino, C. P. Haines, M. Bolzonella, O. Cucciati, A. Gargiulo, B. Granett, J. Krywult, et al.

To cite this version:

M. Siudek, K. Malek, A. Pollo, A. Iovino, C. P. Haines, et al.. Shaping physical properties of galaxy subtypes in the VIPERS survey: Environment matters. Astronomy and Astrophysics - A&A, 2022, 666, 10.1051/0004-6361/202243613 . insu-03863237

HAL Id: insu-03863237

https://insu.hal.science/insu-03863237v1

Submitted on 21 Nov 2022

HAL is a multi-disciplinary open access archive for the deposit and dissemination of scientific research documents, whether they are published or not. The documents may come from teaching and research institutions in France or abroad, or from public or private research centers.

L'archive ouverte pluridisciplinaire **HAL**, est destinée au dépôt et à la diffusion de documents scientifiques de niveau recherche, publiés ou non, émanant des établissements d'enseignement et de recherche français ou étrangers, des laboratoires publics ou privés.

Distributed under a Creative Commons Attribution 4.0 International License

A&A 666, A131 (2022)
https://doi.org/10.1051/0004-6361/202243613
© M. Siudek et al. 2022

Astronomy & Astrophysics

Shaping physical properties of galaxy subtypes in the VIPERS survey: Environment matters★

M. Siudek[1,2], K. Małek[2,3], A. Pollo[2,4], A. Iovino[5], C. P. Haines[6], M. Bolzonella[7], O. Cucciati[7], A. Gargiulo[8], B. Granett[5], J. Krywult[9], T. Moutard[3,11], and M. Scodeggio[10]

[1] Institut de Física d'Altes Energies, The Barcelona Institute of Science and Technology, 08193 Bellaterra, Spain
e-mail: msiudek@ifae.es
[2] National Centre for Nuclear Research, ul. Pasteura 7, 02-093 Warsaw, Poland
[3] Aix Marseille Univ., CNRS, CNES, LAM, Marseille, France
[4] Astronomical Observatory of the Jagiellonian University, ul. Orla 171, 30-244 Kraków, Poland
[5] INAF – Osservatorio Astronomico di Brera, via Brera 28, 20122 Milano, Italy; via E. Bianchi 46, 23807 Merate, Italy
[6] Instituto de Astronomía y Ciencias Planetarias de Atacama (INCT), Universidad de Atacama, Copayapu 485, Copiapó, Chile
[7] INAF – Osservatorio di Astrofisica e Scienza dello Spazio di Bologna, Via Gobetti 93/3, 40129 Bologna, Italy
[8] INAF – Istituto di Astrofisica Spaziale e Fisica Cosmica Milano, Via A. Corti 12, 20133 Milano, Italy
[9] Institute of Physics, Jan Kochanowski University, ul. Swietokrzyska 15, 25-406 Kielce, Poland
[10] INAF – Istituto di Astrofisica Spaziale e Fisica Cosmica Milano, Via Bassini 15, 20133 Milano, Italy
[11] Department of Astronomy & Physics and the Institute for Computational Astrophysics, Saint Mary's University, 923 Robie Street, Halifax, Nova Scotia B3H 3C3, Canada

Received 22 March 2022 / Accepted 27 May 2022

ABSTRACT

Aims. This study aims to explore the relation between the physical properties of different galaxy sub-classes, from red passive to blue star-forming, and their environment. Our work is based on the analysis of 31 631 galaxies from the VIMOS Public Extragalactic Redshift Survey (VIPERS), observed at $0.5 < z < 0.9$. The unprecedented volume of VIPERS and the wealth of auxiliary derived data allow us to associate sub-classes of the main galaxy populations with their possibly different evolutionary paths. This is the first time such a study is performed with such statistical precision.

Methods. We use the results of an unsupervised clustering algorithm to distinguish 11 subclasses of VIPERS galaxies, based on the multi-dimensional feature space, defined by rest-frame UV to NIR colours. We investigate the relationship between the properties of these sub-classes of galaxies and their local environment, defined as the galaxy density contrast, δ, derived from the fifth nearest neighbour technique.

Results. We confirm that the galaxy population-density relation is already in place at $z \sim 0.9$, with the blue galaxy fraction decreasing with density, compensated by an increase in the red fraction. We demonstrate how the properties of red, green, and blue galaxy subclasses are altered as they assemble into denser regions, and we attempt to interpret this in the context of their evolution. On average, red galaxies in the high-density environment are larger by 28% than those in low-density environments. In particular, we find one group of galaxies, sub-class C3, whose increase of size with time can be explained mainly as the result of mergers; for other red subclasses, mergers would not seem to play the major role (subclass C2) or would play a negligible role (sub-class C1). The properties of the green galaxies (sub-classes C4–6) depend on whether their stellar mass is above or below a transition mass, $\log(M_{\rm star}/M_{\odot}) = 10.6$. Low-mass green ($9.5 \lesssim \log(M_{\rm star}/M_{\odot}) \lesssim 10.6$) galaxies appear to have grown through secular processes, while in high-mass ($10.6 \lesssim \log(M_{\rm star}/M_{\odot}) \lesssim 11.5$) green galaxies, mass assembly appears to be dominated by mergers. When it comes to blue galaxies, the trend of decreasing fraction with denser environments seen for the group as a whole (sub-classes C7–11) is found to be driven mostly by one (the most numerous) group of galaxies; sub-class C10. These are compact low-mass galaxies with high, specific star formation rates, which are preferentially found in low-density environments. However, the remaining blue galaxies (sub-classes C7–9) are larger and appear in denser environments than galaxies within C10.

Key words. galaxies: evolution – galaxies: stellar content – galaxies: groups: general

1. Introduction

In the paradigm of hierarchical structure formation, the evolution of the primordial density field acting under gravitational instability drives dark matter to cluster and collapse into virialised objects (haloes). Such haloes provide the potential wells into which baryons fall and galaxies subsequently form (White & Rees 1978). Since we observe different populations of galaxies (spiral, elliptical, irregular) and we know that their distribution in the large scale structure is not random, we can expect the local galaxy density field and/or the properties of the host dark matter halo to influence the evolution of galaxy properties. There are two main possible external factors that affect the evolution of galaxies in the large-scale structure of the Universe: properties of the host dark matter halo (its mass and angular momentum) and interactions with other galaxies. The importance of these two factors is often discussed in the context of

★ Catalog of the galaxies with their class is only available at the CDS via anonymous ftp to cdsarc.u-strasbg.fr (130.79.128.5) or via http://cdsarc.u-strasbg.fr/viz-bin/cat/J/A+A/666/A131

Open Access article, published by EDP Sciences, under the terms of the Creative Commons Attribution License (https://creativecommons.org/licenses/by/4.0), which permits unrestricted use, distribution, and reproduction in any medium, provided the original work is properly cited.
This article is published in open access under the Subscribe-to-Open model. Subscribe to A&A to support open access publication.

the so-called nature vs nurture scenario, where nature corresponds to host dark matter halo properties (Eggen et al. 1962) and nurture to the interactions with other surrounding galaxies (e.g. Toomre & Toomre 1972). It seems to be already clear that the galaxy evolution was driven by a mixture of both factors (e.g. Peng et al. 2010). However, the role of these factors in the evolution of particular populations of galaxies and timescales of the corresponding processes are not yet clear.

Studying relations between the morphology and environment of galaxies in the local Universe, Dressler (1980) found that most elliptical galaxies are located in the densest environments, such as groups and clusters, whereas most spiral galaxies are found in less dense areas. The morphological segregation of galaxies by density appears to be a universal characteristic of galaxy populations (e.g. Balogh et al. 1997; Lewis et al. 2002; Hogg et al. 2003; Kauffmann et al. 2004). Such segregation was confirmed later also beyond the local Universe (e.g. Cucciati et al. 2006, 2017; Tasca et al. 2009; Scoville et al. 2013; Malavasi et al. 2017; Moutard et al. 2018; Laigle et al. 2018; Paulino-Afonso et al. 2019; Sazonova et al. 2020).

The morphology-density relation is tightly correlated with colour (e.g. Poggianti et al. 2008; Skibba et al. 2009; Bait et al. 2017). The existence of such correlations suggests a transformation both in colour and morphology for galaxies in different environments. Up to at least $z \sim 2.5$ massive, bright, red, passive early-type galaxies tend to be more clustered and located in denser environments, while the reverse is true for galaxies that have lower mass, are fainter, bluer, and star-forming (e.g. Cooper et al. 2007; Dressler et al. 1997; Tasca et al. 2009; Chuter et al. 2011; Andreon 2020; Sazonova et al. 2020; Gu et al. 2021). However, colour- and morphology-selected samples are not equal; whilst spirals are mostly blue galaxies and ellipticals are mostly red, a significant fraction of spiral galaxies are red, and many ellipticals are blue (~30%, ~10%, respectively; Smethurst et al. 2022, and references therein). Moreover, the environmental transformation seems to proceed faster from blue to red than the transformation from spiral to elliptical galaxies (e.g. Bamford et al. 2009; Bolzonella et al. 2010).

The morphology-colour-density relation suggests the key role of the environment in regulating the morphological transformation of galaxies accompanied by quenching of their star formation. It is shown in the literature that the number of galaxies and the total stellar mass within the passive galaxy population has grown at least by a factor of two from $z \sim 1$ to $z \sim 0$ (e.g. Bell et al. 2004; Faber et al. 2007). During this process, passive galaxies reveal little or no star formation activity (e.g. Siudek et al. 2017; Sánchez et al. 2019). This implies that, at some point, there should occur a transition of galaxies from the blue star-forming to the red passive population via star formation quenching. Green (intermediate) galaxies are considered to be in transit between blue star-forming and red passive galaxies, and their limited number has been interpreted as a consequence of a fast transformatio *n* process from the former to the latter (e.g. Krywult et al., in prep.; Bell et al. 2004; Schiminovich et al. 2007; Moutard et al. 2016a), or of rejuvenation events (Thomas et al. 2010) from recent infall of the gas. The observed rich panoply of green galaxy morphologies and physical properties suggest the existence of multiple quenching channels (Faber et al. 2007; Moutard et al. 2016a; Pacifici et al. 2016; Siudek et al. 2018a,b) demanding both internal and external processes (e.g. Mahoro et al. 2017; Kelvin et al. 2018).

Taking into account all the complex theories listed above, which do not exhaust all possibilities, dividing galaxies into only two (or three) broad galaxy populations may not be sufficient for comprehensive studies of all aspects of environmental influence on galaxy evolution. Within one galaxy population, there may exist differences in their properties that can be explained by the various mass assembly pathways of blue star-forming and red passive galaxies. For instance, blue galaxies show an intrinsic scatter in the star formation rate-stellar mass relation (e.g. Guo et al. 2013; Matthee & Schaye 2019). Attributing such a scatter to the existence of different sub-classes may reveal the interplay between the various processes that shape how galaxies evolve. This thought led to the idea of adopting methods able to select classes of galaxies, taking into consideration many parameters, and not only the morphology and/or the rest-frame colours, or their estimated star formation activity. In this context, the unsupervised clustering methods can be a valuable approach.

The VIMOS Public Extragalactic Redshift Survey (VIPERS) provides a unique opportunity for environmental studies at intermediate redshifts ($0.5 < z < 1.2$), through a combination of its large volume coverage (comparable to the 2dFGRS in the local Universe) and a well-defined sample of almost 90 000 galaxies, whose global properties and local environments are known. Such large samples are needed to permit the division into multiple statistically representative galaxy sub-populations, which can then be studied and compared. In this paper, we use VIPERS to provide a representative sample of galaxies at $z \sim 0.7$. This unique sample ensures a large number and variety of sources, and provides the multi-wavelength coverage needed to quantify the correlation with the environment. The multi-wavelength coverage of VIPERS and a wealth of auxiliary data were already used to define 11 different sub-classes of galaxies, based on their *UV*-to-*NIR* colours (Siudek et al. 2018a, hereafter S1; see Sect. 2.4). For each VIPERS galaxy, a well-defined environment estimate is available (Cucciati et al. 2017), which was already used to study the environmental effects on the galaxy stellar mass function (Davidzon et al. 2016) and the environment-size relation (Gargiulo et al. 2019).

This paper aims to explore the relationships between different galaxy sub-populations and their environment at $z \sim 0.7$. Our first aim is to show the fraction-density relation for the full galaxy population seen by VIPERS. As a next step, we select (sub)populations that appear promising for more in-depth analysis, which allows the mass-density degeneracy to be broken. In this way, we intend to provide both a possibly comprehensive picture of galaxy type-density dependence at $z > 0.5$, as a starting point, in order to identify galaxy types whose evolutionary paths can be studied in further detail with these or future data. This paper concentrates on relations of the galaxy types defined based on their rest-frame colours; a definition obtained by an automated classification algorithm that combines 12 rest-frame magnitudes from *UV* to *NIR* and local environmental density. Consequently, as our classification was based on colours, the VIPERS galaxy population-density relation reflects the colour rather than the morphology dependence, although the morphological labels are recreated with the accuracy of 0.95 (see Sect. 2.5).

The paper is organised in the following way: in Sect. 2 we present the VIPERS data sample. Section 3 presents the environmental dependence of the fraction of the three main galaxy classes (red, green, and blue). In Sect. 4, we present results for different sub-classes, and we discuss the environmental dependence of red, green, and blue sub-classes in Sects. 5–7, respectively. The summary is presented in Sect. 8. Throughout this paper the cosmological framework with $\Omega_m = 0.30$, $\Omega_\Lambda = 0.70$, and $H_0 = 70\,\mathrm{km\,s^{-1}\,Mpc^{-1}}$ is assumed.

2. Data and sample selection

The data used in this paper are taken from the VIPERS (Scodeggio et al. 2018). VIPERS is a European South Observatory (ESO) large programme performed by the VIMOS spectrograph (VIMOS, Le Fèvre et al. 2003). VIPERS provided spectroscopic redshifts ($z_{\rm spec}$), spectra, and a full photometrically selected parent catalogue for 86 775 galaxies limited to $i_{AB} \leq 22.5$ mag over a total area of ~23.5 deg^2 within the $W1$ (15.7 deg^2) and $W4$ (7.8 deg^2) fields of the Canada-France-Hawaii Telescope Legacy Survey Wide (CFHTLS-Wide). A detailed description of the survey can be found in Guzzo et al. (2014), and Scodeggio et al. (2018). The data reduction pipeline and redshift quality system are described by Garilli et al. (2014). In addition to the spectroscopic information, the VIPERS data value is enhanced by important ancillary information. In particular, morphological parameters are derived by Krywult et al. (2017) and local galaxy densities are measured by Cucciati et al. (2017).

2.1. The physical properties

The physical properties and absolute magnitudes of galaxies were derived from the spectral energy distribution (SED) fitting based on u, g, r, i, and z fluxes from the CFHTLS T0007 release, far-ultraviolet (FUV) and near-ultravilolet (NUV) measurements from the Galaxy Evolution Explorer, near-infrared K_s band from the Wide-field InfraRed Camera, and K from the VISTA Deep Extragalactic Observations survey. The fitting process was performed with the usage of $z_{\rm spec}$, with a grid of stellar population models. The detailed description of the physical parameters (absolute magnitudes, stellar masses, $M_{\rm star}$, and star formation rates, SFR) for the VIPERS sample used in the following analysis can be found in Moutard et al. (2016a). Thanks to the multi-wavelength VIPERS coverage, in the SED fitting we take into account stellar emission, attenuation, and re-emission of stellar emission by interstellar dust, which allows us to robustly recreate the shapes of SEDs. The dependency of the absolute magnitudes on the template library is minimised by using the observed magnitude in the band closest to the redshifted absolute magnitude filter, unless the closest apparent magnitude had an error > 0.3 mag (see Appendix A.1 in Ilbert et al. 2006). Moreover, we are using spectroscopic redshifts, so the physical degeneracies in the redshift-colour space are absent.

2.2. The effective radius

The structural parameters were derived by fitting point spread function (PSF)-convolved Sérsic profiles to the observed i-band CFHTLS-Wide images (Krywult et al. 2017). The fits were performed with GALFIT (Peng et al. 2002), which provides the circularised effective radius, $R_{\rm e}$. The accuracy of the derived parameters was tested on simulated galaxies based on CFHTLS images, returning the uncertainties in $R_{\rm e}$ measurements at the level of 4.4% (12%) for 68% (95%) of the VIPERS sample. A detailed description of the VIPERS morphological parameters can be found in Krywult et al. (2017).

2.3. The environment

As a measure of the environment, we use the VIPERS local density contrast, δ, computed by Cucciati et al. (2017) and defined as:

$$\delta(\mathrm{RA}, \mathrm{Dec}, z) = [\rho(\mathrm{RA}, \mathrm{Dec}, z) - \langle\rho(z)\rangle]/\langle\rho(z)\rangle. \quad (1)$$

Here, $\rho(\mathrm{RA}, \mathrm{Dec}, z)$ is the local density of the tracer centred at the galaxy (RA, Dec, z), and $\langle\rho(z)\rangle$ is the mean density at the tracer's redshift z. The density field is computed using a cylinder with a half-length of $\pm 1000\,\mathrm{km\,s^{-1}}$ and the radius equal to the distance of the fifth nearest neighbour, defined using a subsample of galaxies that trace the density field (tracers).

Tracers were selected from a volume-limited sample that included galaxies with spectroscopic and photometric redshifts. Tracers were selected to satisfy $M_B \leq (-20.4 - z)$, which yields a comoving number density that does not evolve, and therefore is not affected by discreteness effects that change with redshift (Cucciati et al. 2017). With this luminosity limit, the tracer (and our) sample is complete up to $z = 0.9$. A detailed description of the measurements method and environment properties can be found in Cucciati et al. (2014, 2017).

2.4. Galaxy populations

In S1, we selected 52 114 VIPERS objects with the highest confidence (>90%) of redshift measurements and performed their classification into 12 clusters based on the unsupervised machine learning algorithm known as Fisher expectation maximisation (FEM; Bouveyron & Brunet 2011). The FEM method implements a clustering approach called the discriminative latent mixture (DLM) model. It is based on dimensionality reduction as it assumes that data are located in a common low-dimensional latent space. The FEM algorithm iteratively estimates both the discriminative subspace and the parameters of the DLM model. This ensures that improvements to the estimated parameters of the model are adaptive and that the clustering uses only the most important information encoded within the input features. The feature space was defined by spectroscopic redshifts and 12 rest-frame ultraviolet-through-near-infrared magnitudes normalised to the i-band magnitude. The optimal number of clusters was determined using the integrated completed likelihood criterion (ICL; Biernacki et al. 2000), complemented by the physical interpretation of data flow and the properties of clusters. The model revealed substructures in the bimodal colour distribution of galaxies, distinguishing sub-populations of red, green, and blue galaxies. In S1 we verified the ability of FEM to recognise a naturally defined separation in multi-dimensional space, to mirror different mass assembly paths. This new categorisation allowed us to distinguish sub-classes for red, green, and blue galaxy populations, and an additional class of broad-line active galactic nuclei (AGNs), which is discussed in Siudek et al. (in prep.). In the following part, the definition of the red, green, and blue galaxy populations relies on our FEM classification. The red population consists of sub-classes 1–3 (hereafter C1–3), the green population gathers sub-classes 4–6 (hereafter C4–6), and the blue population is created by sub-classes 7–11 (hereafter C7–11).

In particular, sub-classes C1–3 host the reddest spheroidal-shape galaxies that show no sign of star formation activity and are dominated by old stellar populations (as testified by their strong 4000 Å breaks). The inhomogeneity among red sub-classes is expressed mainly in their stellar content traced by UV colours, revealing star formation activity from young hot stars among C3 (see Fig. 2d in Siudek et al. 2018a, and Sect. 5.3). Sub-classes C4–6 host intermediate galaxies whose physical properties, such as colours, sSFR, stellar masses, sizes, and shapes, are intermediate relative to red and blue galaxies. These intermediate galaxies have more concentrated light profiles and lower gas contents than blue galaxies, as per observations of green galaxies in the local Universe

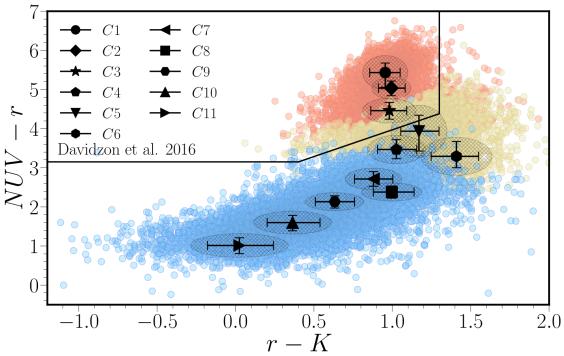

Fig. 1. *NUVrK* diagram of the VIPERS galaxies classified into 11 sub-classes. The median colours of sub-classes are marked with points. The error bars correspond to the 25th and the 75th percentile range of the galaxy colour distribution. The size of ellipses correspond to the normalised median absolute deviation. Galaxies classified as red (C1–3) are separated from the blue galaxies (C7–11) by the solid black line as proposed by Davidzon et al. (2016). Green galaxies (C4–6) are located in between red and blue populations.

(Schiminovich et al. 2007; Schawinski et al. 2014). In particular, the colours of galaxies within C4 suggest that they are dust-free transition galaxies, whereas galaxies within C5 correspond to dustier galaxies, and C6 gathers very dusty star-forming galaxies, potentially edge-on spirals (see Sects. 6.3 and 6.4 for more details). Sub-classes 7–11 contain blue star-forming galaxies. The blue cloud of disk-shaped galaxies means they are actively forming new stars and are populated by young stellar populations (as indicated by the weak 4000 Å break), putting them at a different stage of their evolution. For example, galaxies within C8 are characterised by enhanced star formation activity as indicated by their location on the main sequence plane (see Fig. 7 in Siudek et al. 2018a). Class 11 may consist of low-metallicity galaxies, or AGNs according to their localisation on the AGN diagnostic diagram (see Fig. 10 in Siudek et al. 2018a). The differences between blue sub-classes are further discussed in Sect. 7.3.

Even if such a detailed subdivision is possible only in the multi-dimensional parameter space, it is also well reflected by the NUV–r – r–K diagram (hereafter: $NUVrK$, Arnouts et al. 2013). Figure 1 shows that the three main classes (red, green, and blue) recreate the more standard colour-colour divisions, and they allow for further discrimination of different sub-classes.

For instance, the FEM algorithm distinguishes three sub-classes of VIPERS green galaxies (C4–6) located in between the red and blue populations. Such a multi-wavelength coverage is necessary to unambiguously identify green valley galaxies (S1; Moutard et al. 2020), as different colours yield different bimodalities (e.g. the blue peak of the g–r distribution occupies the green valley of the $NUVrK$ diagram; Salim 2014; Krywult et al., in prep.). Only by considering several colours can substructures contributing to the established bimodalities be uncovered.

Although many applications of unsupervised techniques to various astrophysical analyses have been reported in recent years (see Baron 2019; Ball & Brunner 2010, for reviews), these techniques still pose a number of questions. In particular, applying clustering methods raises the question of whether the cuts in the seemingly continuous distribution of classification feature space reveal genuine clusters, which may be interpreted as distinct galaxy sub-populations. In S1 we addressed these doubts by investigating the non-continuous distribution of features that were not used in the classification scheme throughout different clusters (galaxy sub-classes). In particular, we discussed the comparison between morphological properties: Sérsic index (Sérsic 1963); physical properties: $M_{\rm star}$, SFR; and spectral properties: 4000 Å break, $D4000$, equivalent width of OII line, EW(OII)λ3727, of different sub-classes. This paper shows how the environment varies among the sub-classes of red, green, and blue galaxies, and how they can be connected to different quenching channels.

2.5. The morphological classification

Many studies use colours as the proxy for morphological classifications, assuming that blue colours indicate late-type (disk) galaxies, while red colours are early-type (elliptical) galaxies (Strateva et al. 2001; Park & Choi 2005). As the colour transformation might occur on a shorter timescale than the morphological transformation (e.g. Bamford et al. 2009), the colour-driven classification might be not equal to the morphological one. In S1 we compared FEM classification with a morphological one (Krywult et al. 2017), showing that red galaxies are elliptical galaxies, while blue galaxies correspond to disk galaxies.

To further strengthen the compatibility of our colour-selected galaxy sub-classes with morphology, in this Section we compare our classification with morphological classification from the Dark Energy Survey (DES), which used a supervised deep-learning algorithm (convolutional neural network; Vega-Ferrero et al. 2021). The catalogue was trained on early-type and late-type galaxies with previously known classifications, presented in Domínguez Sánchez et al. (2018), reaching only up to 17.7 mag and their 'emulated' versions at higher redshifts, to extend the magnitude range of the training sample. The test sample (the 'emulated' images with known labels) demonstrated excellent accuracy (~97%) up to 21.5 r-band magnitude, suggesting that the network is able to predict correct morphological types based on the features invisible to the human eye. The comparison sample of 7384 VIPERS galaxies observed up to 21.5 r-band magnitude with DES includes 81% galaxies with secure morphological labels, from which 22% are classified as early-type and 78% as late-type. Early-type galaxies are located mainly within C1–4, not contaminating blue sub-classes (C7–11). At the same time, late-type galaxies dominate in sub-classes C7–11, showing only a very small fraction within sub-classes C1–3. As shown in Vega-Ferrero et al. (2021), 89% of red galaxies (C1–3) are classified as early-type, and 97% of green and blue galaxies (C4–11) as late-type galaxies, which results in an accuracy classification score of ~0.95, defined as the fraction of correctly classified galaxies (see Eq. (5) in Vega-Ferrero et al. 2021). The intermediate sub-classes C4–6 are labelled both as early- and late-type galaxies (with a preference for late-type galaxies). This comparison suggests a strong correlation of colours with morphology for our sample (see Fig. 15 and Sect. 5.3 in Vega-Ferrero et al. 2021, for more details).

2.6. The final sample

In the following analysis, we use the catalogue of 52 114 representative galaxies presented in S1. After excluding 600 broad-line AGNs (mainly assigned to sub-class 12 in S1) and 3966 galaxies with a low probability of belonging to any assigned class (i.e. on the borders between different sub-classes, see details in S1), our sample consists of 47 548 galaxies. We consider only galaxies with reliable δ measurements (i.e. for which at least 60% of the cylinder volume overlaps with the VIPERS survey footprint (gaps and boundaries), see details in

Table 1. Physical properties of the final sample.

Cls	*N*	δ	log(sSFR)	$\log(M_{\rm star})$	$R_{\rm e}$	*n*	*D*4000	*FUV−NUV*
C1	3061	$1.76^{+2.35}_{-1.18}$	$-16.88^{3.55}_{-2.16}$	$10.77^{0.21}_{-0.24}$	$2.38^{+1.33}_{-0.77}$	$3.37^{+1.19}_{-0.97}$	$1.76^{+0.10}_{-0.10}$	$3.16^{0.40}_{-0.45}$
C2	1637	$1.77^{+2.32}_{-1.11}$	$-11.85^{0.29}_{-0.14}$	$10.81^{0.21}_{-0.21}$	$2.91^{+1.36}_{-1.08}$	$3.29^{+1.31}_{-1.05}$	$1.74^{+0.10}_{-0.11}$	$1.60^{0.24}_{-0.22}$
C3	2478	$1.72^{+2.21}_{-1.17}$	$-11.28^{0.37}_{-0.16}$	$10.81^{0.23}_{-0.23}$	$3.00^{+1.29}_{-1.03}$	$3.02^{+1.49}_{-0.97}$	$1.67^{+0.12}_{-0.13}$	$0.83^{0.45}_{-0.27}$
C1–3	7176	$1.75^{+2.29}_{-1.16}$	$-11.99^{0.66}_{-4.45}$	$10.79^{0.22}_{-0.22}$	$2.68^{+1.39}_{-0.92}$	$3.25^{+1.32}_{-1.00}$	$1.73^{+0.10}_{-0.12}$	$1.74^{1.31}_{-0.70}$
C4	2801	$1.43^{+2.00}_{-1.02}$	$-9.73^{0.44}_{-0.63}$	$10.65^{0.22}_{-0.22}$	$3.37^{+1.16}_{-0.96}$	$1.76^{+1.08}_{-0.67}$	$1.41^{+0.14}_{-0.11}$	$1.02^{0.42}_{-0.58}$
C5	2270	$1.46^{+2.09}_{-1.09}$	$-9.57^{0.33}_{-0.17}$	$10.49^{0.22}_{-0.26}$	$2.90^{+1.12}_{-0.86}$	$2.03^{+1.17}_{-0.74}$	$1.49^{+0.16}_{-0.15}$	$2.28^{0.11}_{-0.28}$
C6	688	$1.22^{1.79}_{-0.93}$	$-9.21^{0.38}_{-0.35}$	$10.50^{0.21}_{-0.20}$	$3.77^{+1.26}_{-1.01}$	$1.35^{+0.85}_{-0.51}$	$1.36^{+0.11}_{-0.10}$	$0.71^{0.27}_{-0.45}$
C4–6	5759	$1.42^{2.00}_{-1.04}$	$-9.57^{0.36}_{-0.27}$	$10.57^{0.23}_{-0.24}$	$3.25^{+1.27}_{-0.98}$	$1.77^{+0.98}_{-0.66}$	$1.43^{+0.16}_{-0.12}$	$1.44^{0.80}_{-0.76}$
C7	3281	$1.22^{1.67}_{-0.96}$	$-9.23^{0.44}_{-0.49}$	$10.33^{0.29}_{-0.28}$	$3.48^{+1.19}_{-0.93}$	$1.11^{+0.72}_{-0.38}$	$1.28^{+0.08}_{-0.07}$	$0.79^{+0.55}_{-0.50}$
C8	1203	$1.01^{1.39}_{-0.85}$	$-8.77^{0.27}_{-0.29}$	$10.08^{0.20}_{-0.21}$	$3.32^{+0.93}_{-0.84}$	$0.89^{+0.66}_{-0.31}$	$1.22^{+0.06}_{-0.05}$	$0.21^{+0.16}_{-0.15}$
C9	3468	$0.99^{1.55}_{-0.83}$	$-8.94^{0.37}_{-0.38}$	$9.88^{0.25}_{-0.23}$	$3.11^{+1.09}_{-0.85}$	$0.90^{+0.62}_{-0.28}$	$1.21^{+0.06}_{-0.05}$	$0.78^{+0.28}_{-0.49}$
C10	9207	$0.84^{1.36}_{-0.77}$	$-8.87^{0.30}_{-0.19}$	$9.56^{0.20}_{-0.19}$	$2.96^{+0.90}_{-0.81}$	$0.92^{+0.60}_{-0.30}$	$1.16^{+0.06}_{-0.05}$	$0.21^{+0.26}_{-0.14}$
C11	1537	$0.69^{1.31}_{-0.71}$	$-8.76^{0.37}_{-0.21}$	$9.22^{0.17}_{-0.15}$	$2.51^{+0.96}_{-0.81}$	$1.10^{+0.80}_{-0.45}$	$1.08^{+0.07}_{-0.06}$	$0.07^{+0.19}_{-0.12}$
C7–11	18696	$0.93^{1.44}_{-0.81}$	$-8.93^{0.36}_{-0.29}$	$9.72^{0.34}_{-0.28}$	$3.06^{+0.99}_{-0.84}$	$0.94^{+0.56}_{-0.30}$	$1.18^{+0.07}_{-0.06}$	$0.30^{+0.47}_{-0.21}$

Notes. The number of galaxies (*N*), median values of δ, specific star formation rate, log(sSFR) [yr^{-1}], stellar mass, $\log(M_{\rm star}/M_{\odot})$, effective radius, $R_{\rm e}$ [kpc], Sérsic index, *n*, *D*4000 and rest-frame *FUV−NUV* colour for each sub-class, *Cls*, are provided. Errors correspond to the differences between median and the first and the third quartile, respectively.

Cucciati et al. 2017; Davidzon et al. 2016). This criterion limits our final sample to 31 631 galaxies within the redshift range $0.5 < z < 0.9$. The main physical properties of these galaxies are given in Table 1. For each galaxy, a statistical weight *w* accounting for survey incompleteness is provided. The selection weight, $w = 1/(\mathrm{TSR} \times \mathrm{SSR} \times \mathrm{CSR})$, takes into account three selection functions: the target sampling rate (TSR), the spectroscopic success rate (SSR), and the colour sampling rate (CSR). Further details about these criteria are provided in Garilli et al. (2014) and Scodeggio et al. (2018). The selection weight reflects the representatives of a given galaxy with respect to the underlying parent photometric catalogue. To account for the mass incompleteness introduced by Malmquist bias, each VIPERS galaxy is weighted also by the fraction of the volume in which the galaxy would be still observable (using minimal and maximal redshifts at which it could be observed), following the $1/V_{\rm max}$ method (Schmidt 1968).

For the parts of the analysis that include the size of the galaxy, a further cut on the $R_{\rm e}$ measurement is introduced, leading to a sample of 25 555 galaxies with reliable $R_{\rm e}$ estimates (see Krywult et al. 2017 for details). We claim here that the advantage of our study is the uniquely large galaxy sample over an unprecedented volume, observing 31 631 (25 555 with reliable size measurements) galaxies with spectroscopic redshifts $0.5 < z < 0.9$.

3. The main 3-class separation

In the following sections, we investigate how the fraction of galaxies in different classes vary as a function of the environment. For this reason, we identify four δ bins according to quartiles of the $\log(1 + \delta)$ distribution of the final VIPERS sample. The bottom panel in Fig. 2 shows the distribution of $\log(1 + \delta)$. Since VIPERS is a magnitude-limited survey, we applied corrections (selection and $1/V_{\rm max}$ weights) for survey incompleteness described in Sect. 2.6. We trace the galaxy population-δ relation for red (C1–3), green (C4–6), and blue (C7–11) galaxy classes in two redshift bins.

The upper panel in Fig. 2 shows how the fractions of red, green, and blue galaxies depend on the δ. To verify if we see an evolution of the galaxy population-environment relation, we divided the sample into two redshift bins. To ensure good statistics, we divided the sample at $z = 0.7$, resulting in two redshift bins; 0.5–0.7 and 0.7–0.9, containing 18 259 and 13 372 galaxies, respectively. As Fig. 2 shows, the trends of red, green, and blue galaxies are similar in both our redshift bins, as supported by the agreement of median values in each δ bin for each class in both redshift bins. The choice of the tracer sample (see Sect. 2.3) ensures that densities are not affected by discreteness effects that change with redshift, allowing us to compare the trends in two redshifts bins. However, the direct comparison between fractions of different galaxy classes might still be biased to some extent as the blue galaxy sample is predominantly composed of lower mass galaxies than the red galaxy sample. Similarly, the higher and lower redshift samples have different mass distribution, due to the VIPERS sample selection, which is addressed by adopting the selection and $1/V_{\rm max}$ weights in our sample. We partially address the possible mass incompleteness problem in the following sections by creating a mass-matched sample, which ensures the same $M_{\rm star}$ distribution for the galaxy sub-classes.

Nevertheless, based on Fig. 2 we can safely conclude that in the whole VIPERS redshift range, blue galaxies are more abundant in low-δ environments, while red galaxies prefer denser regions. The blue galaxy fraction steadily decreases from ~70% in the lowest δ bin to ~50% in the high-δ bin. This drop is compensated for by a corresponding rise in the fraction of green and red galaxies. The overall fraction of red galaxies is low but clearly compensates for this trend, increasing their fraction twofold from ~15% to ~30% from the low- to high-δ. At the same time, the increase of the fraction of green galaxies with δ is much flatter, going from ~15% to ~20%. Our results suggest that up to $z \sim 0.9$, red galaxies are preferentially found in denser environments, possibly as a consequence of the fact that in denser environments galaxies form earlier and/or stop their star formation earlier.

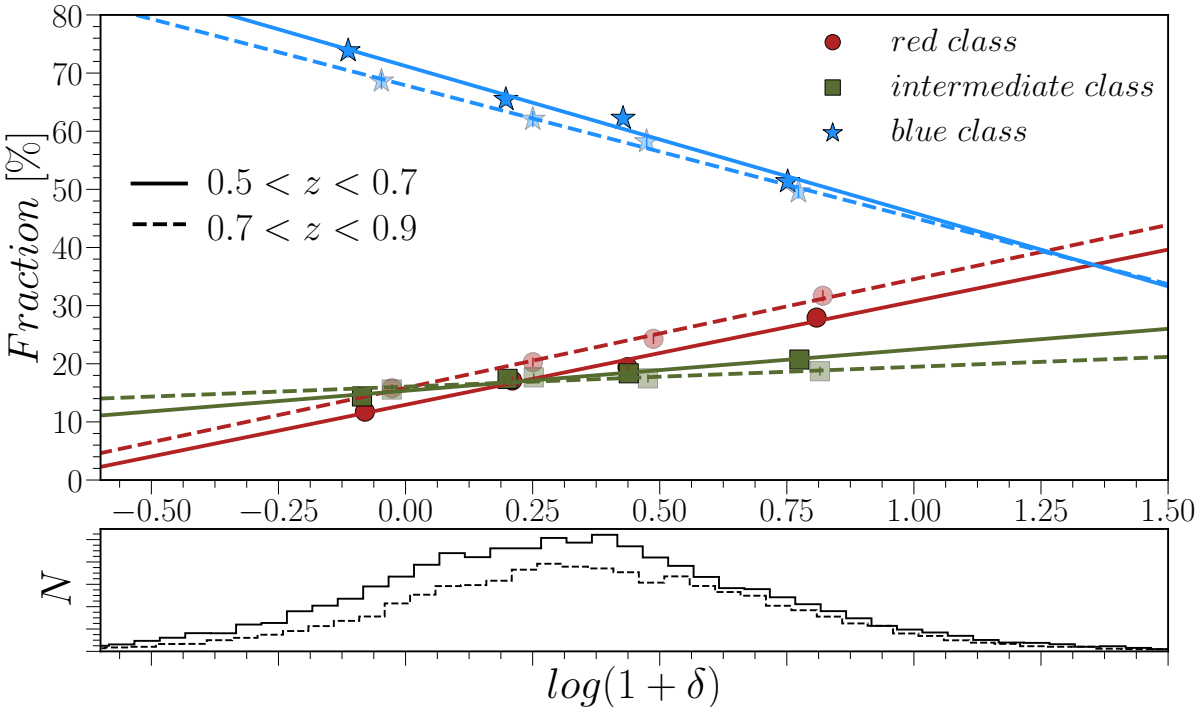

Fig. 2. *Upper panel*: fractions of each VIPERS galaxy population (red, green, and blue) as a function of δ, weighted using selection and $1/V_{\rm max}$ weights. Solid lines correspond to the relation found for redshift range $0.5 < z < 0.7$, whereas dashed lines indicate the dependence of higher-redshift ($0.7 < z < 0.9$) galaxies on environment. *Bottom panel*: distribution of δ for the final sample of 31 631 galaxies. Solid and dashed lines correspond to low- and high-redshift bins, respectively.

Using the COSMOS-ACS data in the redshift range $0.0 < z < 1.2$, Capak et al. (2007) found that the fraction of early-type galaxies increases gradually with δ (especially at $z > 0.4$, see Fig. 10 in Capak et al. 2007). Based on the COSMOS 10k survey, Tasca et al. (2009) explored the evolution of the morphology-δ relation on the sample of 10 644 galaxies up to redshift $z \sim 1$. They found a gradual increasing trend in δ for early-type E/S0 galaxies at redshift $z < 0.5$ and $\log(M_{\rm star}/M_{\odot}) < 10.8$, with the flatter slope for more massive galaxies at higher redshift (see Fig. 7 in Tasca et al. 2009). Paulino-Afonso et al. (2019) confirm the existence of a colour-morphology-δ relation at $z \sim 0.84$, based on the sample of ~500 galaxies from the VIMOS Spectroscopic Survey of a Superstructure in COSMOS. Their results suggest that environment affects colour as well as structure and morphology. As the colour-morphology-δ relation seems to be correlated (see Sect. 1) and our colour classification follows the morphological types (see Sect. 2.5), we claim that our results are in agreement with Capak et al. (2007), Tasca et al. (2009) and Paulino-Afonso et al. (2019). Our results suggest that the environmental dependence of galaxy morphology is tightly correlated with colour, indicating the transformation both in star formation activity and morphology in different environments as it was speculated by, for example, Poggianti et al. (2008), Skibba et al. (2009), Bait et al. (2017), or Paulino-Afonso et al. (2019).

We show that the general trends with the environment are recovered in the population of red and blue galaxies beyond the local Universe. The fraction of green galaxies shows a modest increase (~30%) with δ, much weaker than for red galaxies (~100%), with a fraction of around 15−20%. The low fraction and flat trend is in agreement with the analysis of the Sloan Digital Sky Survey (SDSS) green galaxies presented in Das et al. (2021). Those authors found that the fraction of green galaxies around 10−20% and it does not depend on the environment. Similarly to our sample (see Sect. 2.5), the local green galaxy sample consists mainly (~95%) of spiral (late-type) galaxies.

The modest dependence of the fraction of green galaxies on the δ means that they are found in both low- and high-δ environments, suggesting that either external or internal processes may play an important role in regulating star formation in this population. In Sect. 6 we show that their fractions are dependent on their $M_{\rm star}$.

The comparison of trends in two redshift bins allows us to conclude that the galaxy population-δ relation does not change from redshift 0.5 up to 0.9. As mentioned before, this comparison might still be affected by sample selection bias, which is partially addressed in the following sections by creating a mass-matched sample. The lack of evolution between these two redshift bins indicates that the relation of the galaxy populations (defined by colour) on δ was already largely in place by $z \sim 0.9$. This is in agreement with previous studies showing the existence of such a relation (for galaxies selected by colour or morphology) up to $z \sim 0.9$ (e.g. Cooper et al. 2007; Capak et al. 2007; Tasca et al. 2009; Paulino-Afonso et al. 2019). However, a quantitative comparison with other works is not straightforward due to different classifications, as well as different environment definitions used in the other surveys.

4. The environmental properties of 11 sub-classes

While it is largely accepted that different galaxy populations (defined by their colours or morphologies) preferentially reside in different environments (e.g. Dressler 1980; Balogh et al. 2004; Baldry et al. 2006; Haines et al. 2007; Tasca et al. 2009; Cucciati et al. 2017), it has not yet been shown whether this segregation is related to the galaxy sub-population. Different

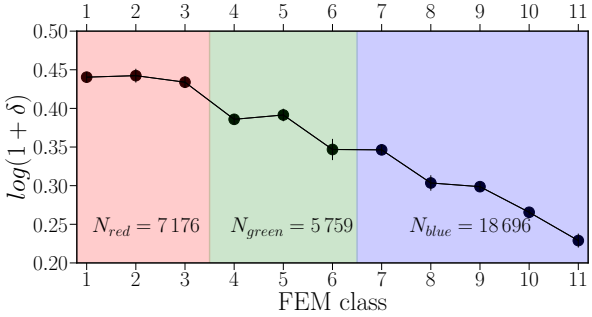

Fig. 3. Median δ for red (C1–3), green (C4–6), and blue (C7–11) galaxies are shown in red, green, and blue, respectively. The error bars correspond to the median absolute deviation. The number of galaxies classified as red, green, and blue are given at the bottom.

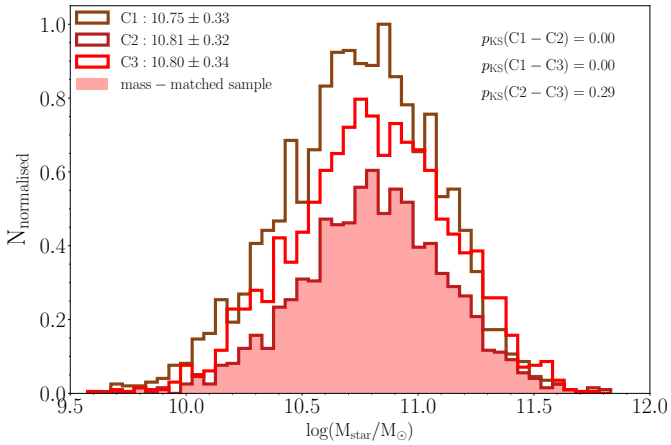

Fig. 4. M_{star} distributions of red sub-classes C1–3 normalised to the maximum value of the histograms. The mean and standard deviation are shown in the upper left. The KS probability is displayed in the upper right. The red filled histogram indicates the M_{star} distribution for the mass-matched sample, which is the same for C1–3.

approaches to the galaxy classification have been proposed, from a visual inspection of small samples, to the automatic clustering algorithms dealing with large galaxy surveys (for review see e.g. Fraix-Burnet et al. 2015), but mostly focused on 2(3)-class categorisation. Taking advantage of the multi-dimensional classification of VIPERS galaxies (presented in S1), in the following sections we show that galaxy sub-populations (sub-classes) show different environmental properties to each other.

In Fig. 3 we show the median δ as a function of the sub-class. As is clearly visible, the sub-classes are strongly correlated with the δ. The general trend indicates that the median δ is decreasing towards the bluest galaxies (i.e. with an increasing number of the sub-class). Sub-classes containing the red galaxies reside in the densest environments, while blue galaxies are found in low-δ regions, with green galaxies located in between. Moreover, we can see that the changes in $\log(1+\delta)$ occur also between different sub-classes of green and blue galaxy populations. The median values of δ together with the main physical properties for 11 sub-classes are given in Table 1 and the distributions of $\log(1+\delta)$ are shown in Appendix A.

In the following sections, we inspect the fraction of galaxies for each sub-class of red, green, and blue population as a function of the environment. If not specified differently, the δ bins correspond to the δ distribution of the whole VIPERS sample and the fraction is given as the number of galaxies in each δ bin over all the galaxies within each sub-class (i.e. for each sub-class, the fractions in δ bins sum up to 100%). This allows us to compare directly the slopes between different sub-classes.

5. Red galaxies

We use our VIPERS sample of 7176 red passive galaxies at redshifts between 0.5 and 0.9 to inspect their environmental dependence. First, we compare M_{star} distribution within C1–3, as the observed environmental trends may be driven by the difference in their masses. As it is clear from Fig. 4, the M_{star} distribution is similar for C1, C2, and C3, as supported also by their median (see Table 1) and mean (reported in the legend) values ($<0.5\sigma$). However, there is a hint of C1 inhabiting slightly less massive galaxies (by 0.04−0.06 dex based on their mean and median values).

To quantify the comparison of the M_{star} distribution for the three red sub-classes, we calculated the two-sample Kolmogorov–Smirnov (KS) null probability for each pair of C1–3 M_{star} distributions, where small values indicate that the two distributions in question are probably not from the same underlying distribution. The outcome of the KS test for C1 (p_{KS} = 0.0007, 0.0003 for sample pairs: (C1, C2) and (C1, C3), respectively) indicates with high probability that C1 and C2 or C3 were not drawn from the same parent population. However, we cannot reject the hypothesis that the mass distributions of C2 and C3 are the same (p_{KS} = 0.29 for sample pair (C2, C3)). Therefore, we create a mass-matched sample by drawing from C1 and C3 a sample that reproduces the same histogram in the M_{star} as C2 (the sample with the lowest number of galaxies in each mass bin), resulting in the total (overall) mass distribution being the same. The mass-matched sample was constructed by separating galaxies into narrow M_{star} bins with a width of 0.05 dex and randomly extracting the same number of galaxies as in the smallest bin.

5.1. The fraction–δ relation

The relation between the fraction of the galaxy sub-class and the environment for C1–3 is shown in Fig. 5. Galaxies within C1–3 follow the general trend found for red galaxies (see Fig. 2), with all three red sub-classes showing a preference to be in a higher δ environment. This preference is similar in strength for all three sub-classes, showing a similar increase by a factor of two between their number in the first and last δ bins (the fraction rises from ~15% to ~35%). The dependence of their fraction on the environment does not seem to be caused by the difference in the M_{star} distribution within C1–3 because the mass-matched sample shows a similar trend (see the bottom panel in Fig. 5). The slopes of the fraction-δ relation are similar for C1–3 (within 1σ), whether we consider the mass-matched sample or not. The trends we find for the red fraction-δ relation (with an average slope of 21.2 ± 1.9) are similar to those (S = 19.4 ± 9.8) found by Cooper et al. (2007) based on the analysis of 76 red galaxies at $0.4 < z < 0.75$ from the DEEP2 galaxy survey.

5.2. The size–δ relation

Before analysing the size–δ relation, we note that C1, C2, and C3 form a sequence of increasing galaxy size, with C1 containing the smallest galaxies (see Table 1). They are ~20% smaller than galaxies within C2 and C3. Even though size was not used as a classification feature, the FEM algorithm used in S1 was

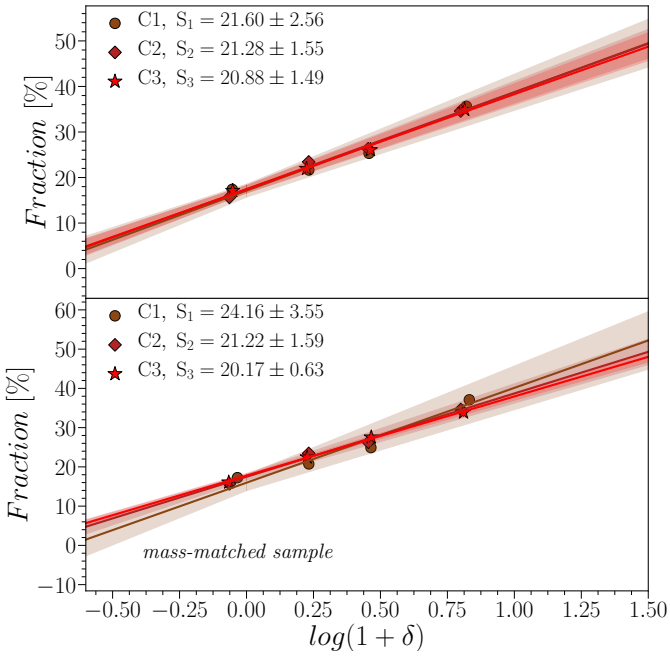

Fig. 5. *Upper panel*: fractions of 3061, 1637, and 2478 red galaxies within C1, C2, and C3, respectively, as a function of the δ. The δ-bins correspond to the quartiles of the δ distribution for the whole sample, and the fractions are normalised to the total number of galaxies in the same sub-class, i.e. for each sub-class the fractions in δ bins sum up to 100%. The solid line corresponds to the weighted fit. The shaded stripes around lines display 1σ of the fit. The error bars correspond to the median absolute deviation on this and all the remaining plots. The slope of the fit is given in the legend. *Bottom panel*: as for the top panel, but for the mass-matched sample. The $M_{\rm star}$ distribution for each red sub-class is the same.

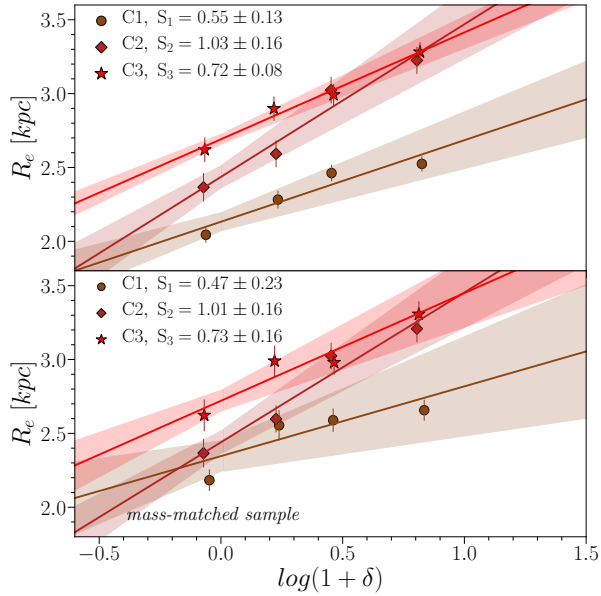

Fig. 6. *Upper panel*: $R_{\rm e}$–δ relation for C1, C2, and C3. The solid line corresponds to the weighted fit. The shaded stripes around lines display 1σ of the fit. The slope of the fit is given in the legend. *Bottom panel*: as for the top panel, but for the mass-matched sample. The $M_{\rm star}$ distribution for each red sub-class is the same.

able to distinguish the cluster (galaxy sub-class), which shows differences also in this property. This suggests that the information about size is incorporated in the galaxy SED and confirms the usefulness of the unsupervised multi-wavelength approach to galaxy classifications.

The dependence of the $R_{\rm e}$ on the δ for C1–3 is shown in Fig. 6. All three sub-classes follow the trend of an increasing $R_{\rm e}$ with denser environments. However, the trend is stronger for galaxies in C2 than for those in C1 and C3, with C1 showing the weakest dependence of the galaxy sizes on the environment. Our findings are independent of whether we use the mass-matched sample or not. This means that even when excluding the less massive galaxies that are overabundant in low-δ environments and usually smaller (Gargiulo et al. 2019) from C1, it does not affect the size–δ relation.

The upwards trend in size–δ correlation is in agreement with other works (e.g. Cooper et al. 2012) and supports the scenario in which the evolution of early-type galaxies at $z < 2$ is triggered in high-δ environments through dry minor mergers. Capak et al. (2007), using data from DEEP2 and DEEP3 surveys, found a similar relation between galaxy size and environment at $z \sim 0.75$, showing that massive early-type galaxies in denser environments are 25% larger than their equal-mass counterparts in lower δ environments. This is consistent with our results as, on average, red galaxies in the high-δ environment are larger by 28% than the ones in low-δ environments for the mass-matched sample.

5.3. Differences between red sub-classes 1–3

C1 consists of the reddest, the most quiescent, the lowest mass, and the smallest galaxies from all three of the red sub-classes (see Table 1 and S1 for a more detailed description). Their $R_{\rm e}$ have a less pronounced dependence on the environment with respect to galaxies within C2 and C3. We claim that dry mergers are not the main driver of the $M_{\rm star}$ accretion of galaxies within C1, in agreement with the analysis of VIPERS massive passive galaxies by Gargiulo et al. (2019), who found no correlation between the surface mean stellar mass density and environment for ~900 massive ($\log(M_{\rm star}/M_\odot) > 11$) passive VIPERS galaxies.

Furthermore, C1 may contain a part of the population of red ultra-compact massive galaxies, known as red nuggets. In Lisiecki et al. (2022), we find 77 red nuggets, of which 49 are found in the C1 sub-class and the rest are distributed among C2–C5. The catalogue of VIPERS ultra-compact massive red galaxies is publicly available (Lisiecki et al. 2022) and their environmental dependence is presented in Siudek et al. (in prep.).

In S1 we showed that C2 contains red galaxies with similar optical colours, $D4000$ strength, and Sérsic indices as galaxies within C1. The main difference in the properties of galaxies within C2, in respect to the ones in C1, is in the level of recent star formation activity, mirrored in a higher specific star formation rate (sSFR) and bluer $FUV-NUV$ colours (see Table 1). Here, we show that galaxies within C2 show the strongest correlation of their $R_{\rm e}$ with the environment (see Fig. 6). Their sizes grow with δ by 36 ± 9% for the mass-matched sample, clearly supporting the hierarchical scenario. It can be explained that galaxies in dense regions evolve faster than galaxies in the field because more mergers occur per unit time in higher densities (e.g. De Lucia et al. 2004; Andreon 2018). This implies that mergers that are efficient in increasing sizes were relevant in the evolution of galaxies within C2.

For galaxies within C3, the $D4000$ strength, optical colours, and Sérsic indices are on a similar level as for galaxies of the two

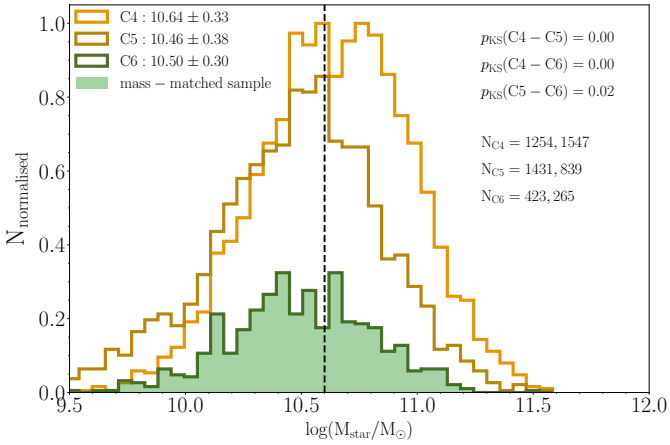

Fig. 7. M_{star} distributions of green sub-classes C4–6 normalised to the maximum value of the histograms. The mean and standard deviation are shown in the upper left. The KS probability is displayed in the upper right. The green filled histogram indicates the M_{star} distribution for the mass-matched sample and corresponds to the area below the distributions for all three sub-classes. The vertical line corresponds to the transition mass at $z \sim 0.7$. The number of galaxies in low- and high-mass samples, respectively for each sub-class, are given in the centre-right.

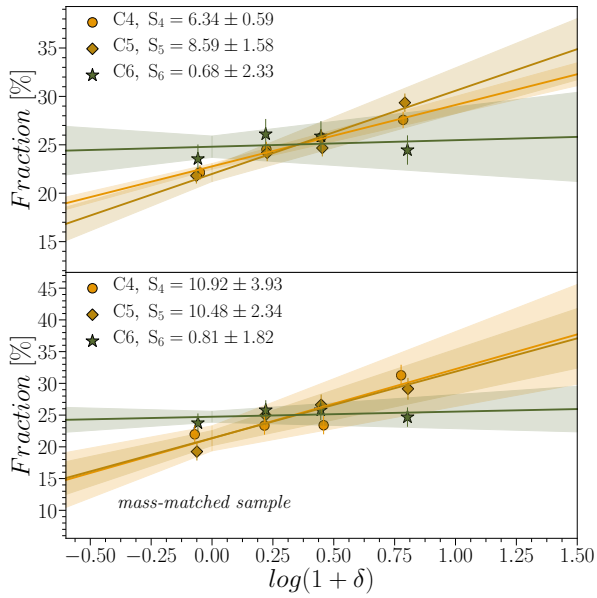

Fig. 8. *Upper panel*: fractions of 2801, 2270, and 688 green galaxies within C4, C5, and C6, respectively, as a function of the δ. The δ-bins correspond to the quartiles of the δ distribution for the whole sample, and the fractions are normalised to the total number of galaxies in the same sub-class, i.e. for each sub-class the fractions in δ bins sum up to 100%. The solid line corresponds to the weighted fit. The shaded stripes around lines display 1σ of the fit. The slope of the fit is given in the legend. *Bottom panel*: as for the top panel, but for the mass-matched sample. The M_{star} distribution for each green sub-class is the same.

remaining red sub-classes. However, galaxies within C3 show the highest sSFR and the bluest $FUV-NUV$ colours among red sub-classes (see Table 1), which may indicate that the star formation activity contributes more to C3 than to the C1 and C2 (see S1 for details). C3 tends to contain the largest red galaxies, especially in low-δ environments in respect to C1 and C2 (see Fig. 6 and Table 1). The correlation of properties of galaxies within C3 with the environment is in between those found for C1 and 2. This may imply that dry mergers occur among those galaxies, but it is not the only or the main ingredient of their star formation history (SFH).

6. Green galaxies

In this section, using a sample of 5759 green galaxies at redshift $0.5 < z < 0.9$, we investigate their environmental properties and dependence on the M_{star}. Similarly to red galaxies (see Sect. 5), we first verified the difference in M_{star} distributions within C4–6, which seem to be similar for each green sub-class as shown in Fig. 7 and supported also by their median (see Table 1) and mean values (see the legend). Their M_{star} distributions are in agreement within 0.5σ, but their mean and median values form a sequence of decreasing values, which underline different distributions confirmed by the KS test (with $p \sim 0$), indicating with high probability that their M_{star} is not drawn from the same parent sample. To account for the differences in mass distributions, we create a mass-matched sample following the methodology introduced for red galaxies (see Sect. 5).

6.1. The fraction-δ relation

As is clear from Fig. 2, the fraction of green galaxies is low, showing a small increase towards denser environments. In Fig. 8 we plot the fraction–δ relation for the green sub-classes C4–6. We can see that the trend observed in Fig. 2 is driven by C4 and C5. The trend of the relation for C6 is flat ($0.8 \pm 1.8\%$ for the mass-matched sample), whereas for C4 and C5 it is significantly sharper ($10.7 \pm 3.1\%$). However, it is still weaker by a factor of two than the one found for red sub-classes ($21.9 \pm 1.9\%$ for the mass-matched sample). The fraction-δ relation seems to be independent of differences in the M_{star} distributions within C4–6, as the mass-matched sample shows the same trend (see the bottom panel in Fig. 8).

6.2. The size–δ relation

Galaxies within C6 are the largest, while the galaxies within C5 are the smallest, placing C4 galaxies in between (see Table 1). The median size of the galaxies within C5 is similar to the median size of those within red C2–3, while the galaxies in C6 are larger by ~36% than those in the red population, and even larger than those in the blue population (by ~23%). Although the sizes of green galaxies within the three sub-classes are different, the dependence of their sizes on the environment is similar. The size–δ relation is shown in Fig. 9. All three green sub-classes follow the trend of the mildly increasing R_e with δ ($0.7 \pm 0.1\%$), which is similar to the trend found for red galaxies ($0.8 \pm 0.1\%$). The size dependence for all three sub-classes is in agreement within 1σ. However, their size is dependent on their M_{star}, as the more massive galaxies are larger (R_e is smaller for the mass-matched sample, which removes the excess of high-mass galaxies). For the mass-matched sample of all three sub-classes, the size weakly (~7−15%) rises from low- to high-densities with a similar strength (~0.5σ).

6.3. Differences between green sub-classes

Galaxies within C6 differ from the ones in C4–5, as they are the largest galaxies within our sample ($R_e \sim 3.77$ kpc, see Table 1), including the blue sub-classes. At the same time, they are relatively massive with reduced star formation (see Table 1). Its

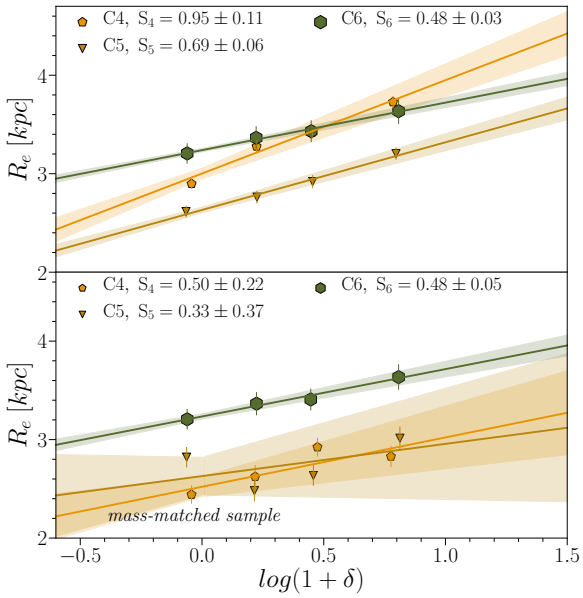

Fig. 9. *Upper panel*: R_e–δ relation for the three green galaxy sub-classes C4–6. The solid line corresponds to the weighted fit. The shaded stripes around lines display the 1σ uncertainty of the fit. *Bottom panel*: as for the top panel, but for the mass-matched sample. The M_{star} distribution for each green sub-class is the same.

location on the $NUVrK$ diagram (see Fig. 1) in particular is consistent with previous descriptions of the edge-on galaxies (Arnouts et al. 2013; Moutard et al. 2016b). Their red $r - K$ colours may be a consequence of dust within the disks or their high inclination. The presence of the prominent disk may also explain their low Sérsic indices (with a median of $n = 1.35$) in comparison with those of the red population ($n > 3$, see Table 1). This suggests that C6 contains spiral galaxies, possibly including dust reddened candidates. Those galaxies occupy less dense environments (with respect to red galaxies and the remaining green subclasses, see Table 1), and their fraction does not depend on the environment. This suggests that their evolution is dominated rather by internal processes, such as mass quenching, in which stellar and/or AGN feedback removes gas from the galaxies, while bulges stabilise their disks against collapse, which inhibits star formation. The dominance of galaxies within C4–5 in denser environments suggests that those galaxies are on a different evolutionary pathway, preferentially dominated by external processes that move these galaxies onto the red sequence over time.

6.4. The transition mass

The green sub-classes mostly contain galaxies with M_{star} close to the so-called transition mass ($\log(M_{cross}/M_\odot) = 10.6$ at $z \sim 0.7$; Davidzon et al. 2013, see Fig. 7), where the mass functions of the star-forming and passive galaxies cross (above the transition mass the red population dominates, while below that mass, the blue cloud is the most numerous population). This sharp transition in M_{star} reflects the differences in the evolution of low- and high-mass galaxies (Haines et al. 2007). Low-mass galaxies with shallower potential wells are characterised by more extended star formation histories and longer gas-consumption timescales (van Zee 2001), while massive galaxies with deeper potential wells consume their gas in a short burst (<2 Gyr; Chiosi & Carraro 2002). In particular, this transition in galaxy properties with mass may be explained by the transition from cold to hot gas accretion modes when galaxy haloes reach a mass of $\sim 10^{12}$ (Dekel & Birnboim 2006).

The fractions of green galaxies divided according to the transition mass are shown in Fig. 10. As there are no noticeable differences in the fraction-δ relations whether we consider mass-matched samples or not, we show plots only for the mass-matched samples. In each panel, the green fraction as a function of the environment is given in two M_{star} bins for the three green sub-classes combined (C4–6) and C4–6 separately.

Overall, green galaxies show a trend in M_{star} (transition mass) that may be correlated to downsizing. The low-mass green galaxies are defined here as those with $9.5 \lesssim \log(M_{star}/M_\odot) \lesssim 10.6$ (see Fig. 7). Our studies, however, do not extend to the dwarf regime ($\log(M_{star}/M_\odot) \lesssim 9.5$), whose galaxies are expected to be differently affected by environment (e.g. Guo et al. 2017; Moutard et al. 2018) than more massive galaxies. Green galaxies are not star forming anymore (in fact they are intermediate) and their fraction tends to be flat with δ. The lack of trend in δ suggests that low-mass green galaxies are not undergoing environmental quenching.

Figure 10 shows that high-mass green galaxies have a strong preference towards high-δ regions, irrespective of sub-class. This suggests that environmental quenching is primarily responsible for producing these high-mass green galaxies. Moutard et al. (2016a) show that the high-mass green galaxies took longer to transit (pass through the green valley) than the low-mass green valley galaxies. This interpretation is supported by Haines et al. (2013), who find a large number of transition galaxies (with SFRs reduced by a factor of two to three) in clusters whose quenching occurs slowly (on 1–2 Gyr timescales). The increasing trend in the fraction of massive green galaxies with increasing δ is also consistent with the hypothesis of merger-driven evolution of massive green valley galaxies discussed in Moutard et al. (2020). The authors find that massive galaxies that are already in the process of quenching (i.e. green massive galaxies) host heavily obscured X-ray AGNs. This is consistent with a quenching scenario that involves major mergers.

7. Blue galaxies

The FEM classification yields five blue star-forming sub-classes, which catch the blue population at different parts along the galaxy main star-forming sequence (see Sect. 4.3 in S1). However, S1 found that C11 contained many narrow-line AGNs, so we do not consider C11 in the remaining analysis, and we discuss the environmental properties of this sub-class in Siudek et al. (in prep.).

Figure 11 shows the M_{star} distributions for C7–10. Following the approach introduced in Sect. 5, we create the mass-matched sample to check if the relation of the number or properties of blue sub-classes depends on the different M_{star} distributions among C7–10. Blue sub-classes are characterised by different mass distributions, as also confirmed by KS tests, and their median (see Table 1) and mean values (see the legend in Fig. 11). The mass-matched sample of 3784 blue galaxies returns the same M_{star} distribution for C7–10 and allows us to directly compare the trends in the fraction-δ relations between the different sub-classes.

7.1. The fraction-δ relation

The strong trend in the decreasing fraction of blue galaxies with a denser environment, visible in Fig. 2, is driven mainly by one

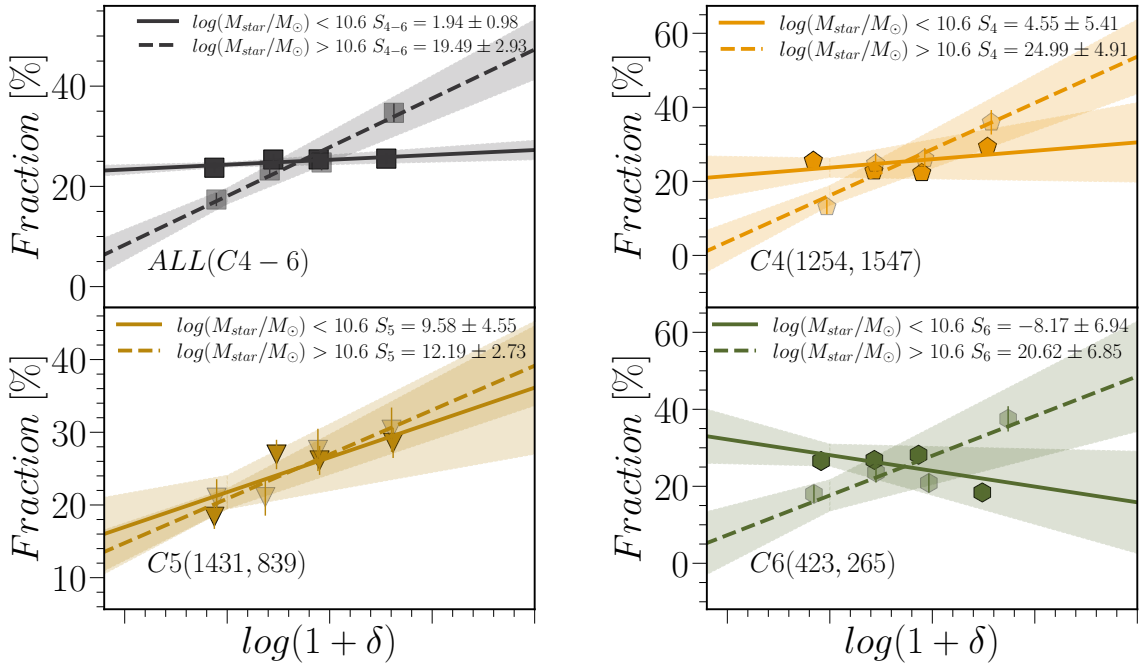

Fig. 10. In each panel, the fraction of the mass-matched sample of green galaxies, divided according to the transition mass as a function of the environment, is given for the three green sub-classes combined (C4–6) and separately (C4, C5, and C6). The δ-bins correspond to the quartiles of the δ distribution for the whole sample, and the fractions are normalised to the total number of galaxies in the same sub-class, i.e. for each sub-class the fractions in δ bins sum up to 100%. The solid and dashed lines correspond to the weighted fit for low- ($9.5 \lesssim \log(M_{\rm star}/M_\odot) \lesssim 10.6$) and high-mass ($10.6 \lesssim \log(M_{\rm star}/M_\odot) \lesssim 11.5$) relations, respectively. The shaded stripes around lines display 1σ of the fit. The slope of the fit is given in the legend. The number of galaxies in low- and high-mass samples, respectively for each sub-class, are given in parenthesis.

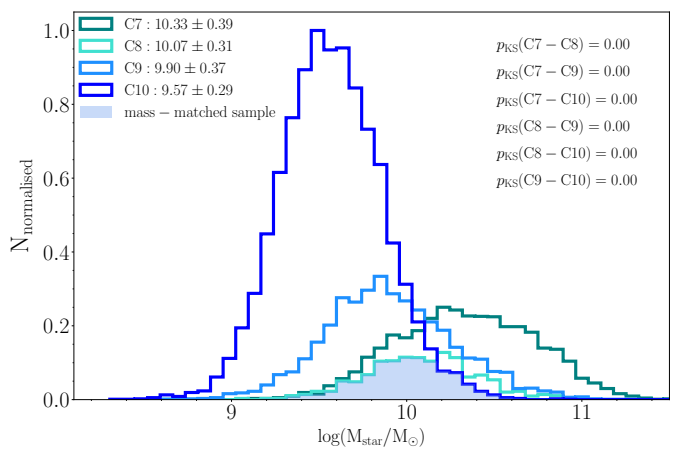

Fig. 11. $M_{\rm star}$ distributions of blue sub-classes C7–10 normalised to the maximum value of the histograms. The mean and standard deviation are shown in the upper left. The KS probability is displayed in the upper right. The blue filled histogram indicates the $M_{\rm star}$ distribution for the mass-matched sample and corresponds to the area below the distributions for all sub-classes. The mass-matched sample returns the same $M_{\rm star}$ distribution for all four C7–10 sub-classes.

(the most numerous) sub-class; C10 (see Fig. 12). The environmental dependence of the fraction of C7–9 is at least twice as weak as the one for C10, with C7 showing an almost flat trend. This may imply that around a half of the blue cloud population at $z \sim 0.7$, gathered in C10 (see Table 1), follow the same, most likely mass-driven, secular SFH. The remaining classes contain star-forming galaxies evolving under a combination of mass-dependent secular SFH and other physical processes, which lead to the lack of a strong correlation with the environment.

Contrary to the behaviour of red and green sub-classes, the blue sub-class shows stronger dependence of the fraction-δ relation on the $M_{\rm star}$ distribution (see Figs. 5, 8, and 12 for the trends found for red, green, and blue sub-classes, respectively). The differences in stellar mass distributions of blue sub-classes suggest that the low-mass ($\log(M_{\rm star}/M_\odot) < 10$) blue galaxies are the ones responsible for the strong decreasing trend of the fraction-δ relation (i.e. the dense-environment is penalising the survivors of low-mass galaxies).

7.2. The size-δ relation

The size as a function of δ for blue sub-classes C7–10 is shown in Fig. 13. In the upper panel in Fig. 13 we can see that, on average, $R_{\rm e}$ of galaxies gathered in C10 is smaller and the trend of the increasing size with a denser environment is weaker than for galaxies within C7–9. $R_{\rm e}$ of galaxies within C7–9 are increasing, on average, three times more than those of galaxies in C10 when moving from low- to high-δ environments (i.e. $R_{\rm e}$ increases ~15% from the lowest to the highest δ percentile for galaxies within C7–9, and only ~5% within C10).

To verify if the difference in environmental trends of $R_{\rm e}$ that we see between C7–9 and C10 are reflecting their different $M_{\rm star}$ distributions, we consider a mass-matched sample (see the bottom panel of Fig. 13). The milder dependence of $R_{\rm e}$ on the environment for the mass-matched sample for C10 than for C7–9 may reflect that C10 gathers star-forming compact galaxies with the lowest $M_{\rm star}$ and even when found in high-δ environments, they remain small. Haines et al. (2007) showed that the effect of the environment on galaxy evolution increases when moving from high-mass to low-mass galaxies. Higher-mass star-forming

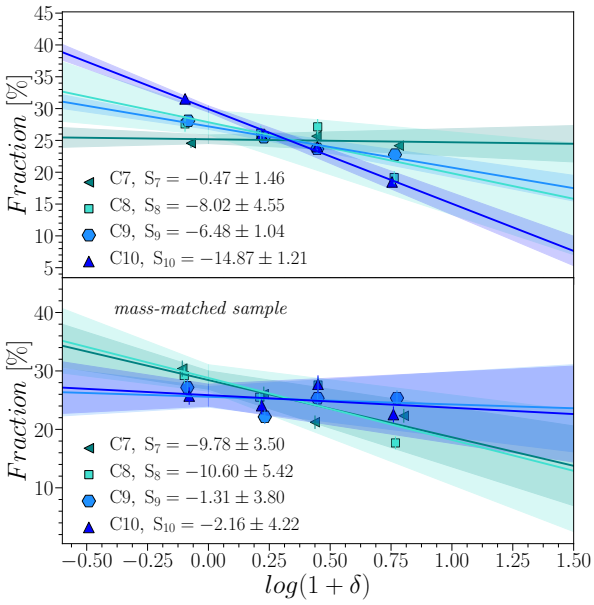

Fig. 12. *Upper panel*: the fractions of 3281, 1203, 3468, and 9207 blue galaxies within C7, C8, C9, and C10, respectively, as a function of the δ. The δ-bins correspond to the quartiles of the δ distribution for the whole sample and the fractions are normalised to the total number of galaxies in the same sub-class, i.e. for each sub-class, the fractions in δ bins sum up to 100%. The solid line corresponds to the weighted fit. The shaded stripes around lines display 1σ of the fit. The slope of the fit is given in the legend. *Bottom panel*: as for the top panel, but for the mass-matched sample. The $M_{\rm star}$ distribution for each blue sub-class is the same.

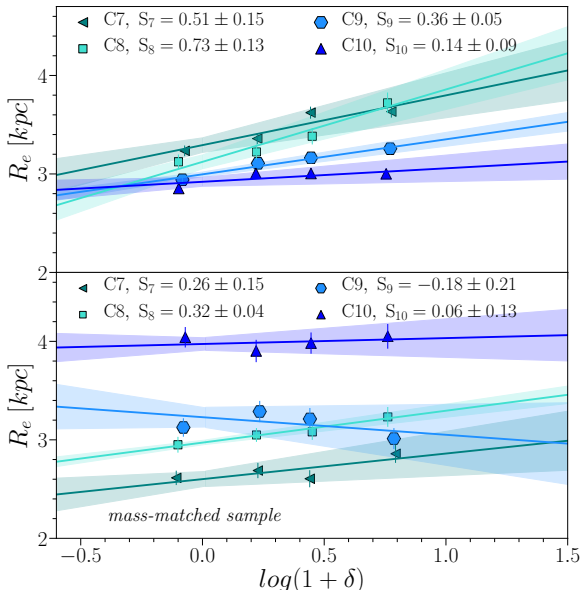

Fig. 13. *Upper panel*: dependence of the $R_{\rm e}$ on the δ for four blue galaxy sub-classes. The solid line corresponds to the weighted fit. Shaded stripes around lines display the 1σ uncertainty of the fit. *Bottom panel*: as for the top panel, but for the mass-matched sample. The $M_{\rm star}$ distribution for each blue sub-class is the same.

galaxies are more resistant to external environmental processes than lower mass star-forming galaxies, and also evolve secularly (along the main star-forming sequence) earlier than dwarf galaxies.

We can clearly see that the smaller $R_{\rm e}$ found for the galaxies in C10 (see upper panel in Fig. 13) were driven by lower mass galaxies. As for the mass-matched sample (lower panel), C10 gathers the largest galaxies (with respect to remaining sub-classes) with no signs of preference of the size of galaxies on the environment. This means that half of the blue population (i.e. sub-class C10) are compact low-mass galaxies preferentially residing in low-δ environments, but not showing different properties if found in denser regions.

7.3. Differences between blue sub-classes

Galaxies within C10 seem to be the star-forming galaxies that may follow the early, fast quenching channel described by Moutard et al. (2016b; 2018; see their Fig. 3a). Young, low-mass quiescent galaxies with bluer $r - K$ (<0.76) colours must have followed this fast quenching channel. This population of young quiescent galaxies is heavily affected and/or discarded by the double selection of VIPERS ($i < 22.5$ and $z > 0.5$), and thus the FEM algorithm was not able to distinguish them as a separate sub-class. However, their star-forming progenitors seem to be gathered in C10.

Galaxies gathered in C10 are relatively low-mass ($\log(M_{\rm star}/M_\odot) \sim 9.56$) and small ($R_{\rm e} \sim 2.96$ kpc). They have relatively high sSFR and preferentially reside in low-δ environments (see Table 1). This suggests that the most compact star-forming galaxies with high sSFRs are preferentially quenched in dense environments. This is in line with recent studies that galaxies with very high star formation activity are strongly depleted in dense environments because of the rapid environmental quenching (stellar feedback and the stripping of the extended halo), becoming post-starburst galaxies (Socolovsky et al. 2018, 2019).

C7–9 may contain galaxies with different evolution mechanisms than the most populated C10. The sSFRs are lower than for galaxies within C10, consistent with the hypothesis that they fade as time passes. The sSFR was shown to depend on the environment, and on average, is lower in denser regions, which may be attributed to a lower fraction of star-forming galaxies in a denser environment (e.g. Peng et al. 2010; Darvish et al. 2016) and a lower star formation activity (~0.1−0.3 dex) of star-forming galaxies in denser environments than the field (e.g. Vulcani et al. 2010; Haines et al. 2013; Darvish et al. 2017). At the same time, galaxies within C7–9 are larger than those from the blue population in C10 (see Table 1), showing a larger dependence of their sizes on the environment. However, for the mass-matched sample the effect is opposite; galaxies within C10 are larger than those in C7–9. The observed trend might imply that higher mass, larger galaxies can continue forming stars longer in hostile environments. Haines et al. (2017) show that larger galaxies can continue to form stars to higher stellar masses than smaller galaxies. That would suggest that the process of star formation is favoured or more resilient in more diffuse or less compact galaxies.

8. Summary

We analyse the relations between the physical properties of galaxy (sub)classes and their δ, based on a sample of 31 631 VIPERS galaxies observed over the redshift range $0.5 < z < 0.9$.

In agreement with previous studies (Capak et al. 2007; Tasca et al. 2009; Cucciati et al. 2017; Paulino-Afonso et al. 2019), we find that the galaxy population-δ relation is already at place at $z \sim 0.9$. Based on the VIPERS sample, which has a statistical fidelity comparable to local surveys such as the SDSS but peaks at $z \sim 0.7$, we confirm that in the whole analysed redshift range ($0.5 < z < 0.9$) the main trends seen in the local Universe (e.g. Balogh et al. 2004; Baldry et al. 2006; Haines et al. 2007), are already present (see Fig. 2). The fraction of red passive galaxies increases with δ, while the fraction of blue star-forming galaxies decreases with an increasing δ. At the same time, red galaxies in a high-δ environment are 28% larger than the ones in low-dense environments for the mass-matched sample. The galaxy population-δ relations at $0.7 < z < 0.9$ and $0.5 < z < 0.7$ are remarkably similar, suggesting that the processes correlated with environment played their role to establish these trends at redshift higher than 1.

The more detailed classification allows us to have deeper insights into the influence of the environment on the properties of different populations of galaxies. We make use of the classification based on the unsupervised clustering method performed by Siudek et al. (2018a), which subdivided the red, green, and blue galaxy populations in VIPERS into 11 sub-classes to test the hypothesis that these subclasses may be related to different evolutionary paths inside the three main galaxy populations. The most relevant findings are:

- All three red sub-classes (C1–C3) show the same preference for denser environments, but their sizes differ and correlate with the local environment in different ways, suggesting that dry merger activity mostly shaped galaxies within C3, while galaxies within C1 were quenched mostly as a result of internal processes.
- High-mass ($\log(M_{\rm star}/M_{\odot}) > 10.6$) green galaxies (C4–6) are driving the positive fraction-density relation found for the intermediate galaxies, suggesting that environmental quenching is more important in the evolution of high-mass green galaxies.
- The majority of blue galaxies (C10) follow the decreasing trend of the fraction-density relation, following genuine passive evolution through accretion of the surrounding gas.

Our study confirms that the separation of galaxies into red, green, and blue populations is insufficient to recreate the full panoply of galaxies and their different environmental trends. The application of unsupervised machine-learning techniques working in a multi-dimensional feature space allows us to discover new patterns and automatically identify rare (peculiar) galaxy populations as red nuggets (Lisiecki et al. 2022) or AGNs in dwarf galaxies (Siudek et al., in prep.).

Acknowledgements. The authors want to thank Bianca Garilli, Luigi Guzzo and the referee for useful and constructive comments. This work has been supported by the European Union's Horizon 2020 Research and Innovation programme under the Maria Sklodowska-Curie grant agreement (No. 754510), the Polish National Science Centre (UMO-2016/23/N/ST9/02963, and UMO-2018/30/M/ST9/00757), the Spanish Ministry of Science and Innovation through the Juan de la Cierva-formacion programme (FJC2018-038792-I), and by Polish Ministry of Science and Higher Education grant DIR/WK/2018/12. K.M. has been supported by the National Science Centre (UMO-2018/30/E/ST9/00082). C.P.H. acknowledges support from ANID through Fondecyt Regular 2021 project no. 1211909.

References

Andreon, S. 2018, A&A, 617, A53
Andreon, S. 2020, A&A, 640, A34
Arnouts, S., Le Floc'h, E., Chevallard, J., et al. 2013, A&A, 558, A67
Bait, O., Barway, S., & Wadadekar, Y. 2017, MNRAS, 471, 2687
Baldry, I. K., Balogh, M. L., Bower, R. G., et al. 2006, MNRAS, 373, 469
Ball, N. M., & Brunner, R. J. 2010, Int. J. Mod. Phys. D, 19, 1049
Balogh, M. L., Morris, S. L., Yee, H. K. C., Carlberg, R. G., & Ellingson, E. 1997, ApJ, 488, L75
Balogh, M. L., Baldry, I. K., Nichol, R., et al. 2004, ApJ, 615, L101
Bamford, S. P., Nichol, R. C., Baldry, I. K., et al. 2009, MNRAS, 393, 1324
Baron, D. 2019, ArXiv e-prints [arXiv:1904.07248]
Bell, E. F., Wolf, C., Meisenheimer, K., et al. 2004, ApJ, 608, 752
Biernacki, C., Celeux, G., & Govaert, G. 2000, IEEE Trans. Pattern Anal. Mach. Intell., 22, 719
Bolzonella, M., Kovač, K., Pozzetti, L., et al. 2010, A&A, 524, A76
Bouveyron, C., & Brunet, C. 2011, Statistics and Computing, 22, 301
Capak, P., Abraham, R. G., Ellis, R. S., et al. 2007, ApJS, 172, 284
Chiosi, C., & Carraro, G. 2002, MNRAS, 335, 335
Chuter, R. W., Almaini, O., Hartley, W. G., et al. 2011, MNRAS, 413, 1678
Cooper, M. C., Newman, J. A., Coil, A. L., et al. 2007, MNRAS, 376, 1445
Cooper, M. C., Griffith, R. L., Newman, J. A., et al. 2012, MNRAS, 419, 3018
Cucciati, O., Iovino, A., Marinoni, C., et al. 2006, A&A, 458, 39
Cucciati, O., Granett, B. R., Branchini, E., et al. 2014, A&A, 565, A67
Cucciati, O., Davidzon, I., Bolzonella, M., et al. 2017, A&A, 602, A15
Darvish, B., Mobasher, B., Sobral, D., et al. 2016, ApJ, 825, 113
Darvish, B., Mobasher, B., Martin, D. C., et al. 2017, ApJ, 837, 16
Das, A., Pandey, B., & Sarkar, S. 2021, JCAP, 2021, 045
Davidzon, I., Bolzonella, M., Coupon, J., et al. 2013, A&A, 558, A23
Davidzon, I., Cucciati, O., Bolzonella, M., et al. 2016, A&A, 586, A23
Dekel, A., & Birnboim, Y. 2006, MNRAS, 368, 2
De Lucia, G., Poggianti, B. M., Aragón-Salamanca, A., et al. 2004, ApJ, 610, L77
Domínguez Sánchez, H., Huertas-Company, M., Bernardi, M., Tuccillo, D., & Fischer, J. L. 2018, MNRAS, 476, 3661
Dressler, A. 1980, ApJ, 236, 351
Dressler, A., Oemler, A., Jr., Couch, W. J., et al. 1997, ApJ, 490, 577
Eggen, O. J., Lynden-Bell, D., & Sandage, A. R. 1962, ApJ, 136, 748
Faber, S. M., Willmer, C. N. A., Wolf, C., et al. 2007, ApJ, 665, 265
Fraix-Burnet, D., Thuillard, M., & Chattopadhyay, A. K. 2015, Front. Astron. Space Sci., 2, 3
Gargiulo, A., Cucciati, O., Garilli, B., et al. 2019, A&A, 631, A15
Garilli, B., Guzzo, L., Scodeggio, M., et al. 2014, A&A, 562, A23
Gu, Y., Fang, G., Yuan, Q., Lu, S., & Liu, S. 2021, ApJ, 921, 60
Guo, K., Zheng, X. Z., & Fu, H. 2013, ApJ, 778, 23
Guo, Y., Bell, E. F., Lu, Y., et al. 2017, ApJ, 841, L22
Guzzo, L., Scodeggio, M., Garilli, B., et al. 2014, A&A, 566, A108
Haines, C. P., Gargiulo, A., La Barbera, F., et al. 2007, MNRAS, 381, 7
Haines, C. P., Pereira, M. J., Smith, G. P., et al. 2013, ApJ, 775, 126
Haines, C. P., Iovino, A., Krywult, J., et al. 2017, A&A, 605, A4
Hogg, D. W., Blanton, M. R., Eisenstein, D. J., et al. 2003, ApJ, 585, L5
Ilbert, O., Arnouts, S., McCracken, H. J., et al. 2006, A&A, 457, 841
Kauffmann, G., White, S. D. M., Heckman, T. M., et al. 2004, MNRAS, 353, 713
Kelvin, L. S., Bremer, M. N., Phillipps, S., et al. 2018, MNRAS, 477, 4116
Krywult, J., Tasca, L. A. M., Pollo, A., et al. 2017, A&A, 598, A120
Laigle, C., Pichon, C., Arnouts, S., et al. 2018, MNRAS, 474, 5437
Le Fèvre, O., Saisse, M., Mancini, D., et al. 2003, in Society of Photo-Optical Instrumentation Engineers (SPIE) Conference Series, eds. M. Iye, & A. F. M. Moorwood, 4841, 1670
Lewis, I., Balogh, M., De Propris, R., et al. 2002, MNRAS, 334, 673
Lisiecki, K., Malek, K., & Siudek, M. 2022, A&A, submitted
Mahoro, A., Pović, M., & Nkundabakura, P. 2017, MNRAS, 471, 3226
Malavasi, N., Pozzetti, L., Cucciati, O., et al. 2017, MNRAS, 470, 1274
Matthee, J., & Schaye, J. 2019, MNRAS, 484, 915
Moutard, T., Arnouts, S., Ilbert, O., et al. 2016a, A&A, 590, A103
Moutard, T., Arnouts, S., Ilbert, O., et al. 2016b, A&A, 590, A102
Moutard, T., Sawicki, M., Arnouts, S., et al. 2018, MNRAS, 479, 2147
Moutard, T., Malavasi, N., Sawicki, M., Arnouts, S., & Tripathi, S. 2020, MNRAS, 495, 4237
Pacifici, C., Kassin, S. A., Weiner, B. J., et al. 2016, ApJ, 832, 79
Park, C., & Choi, Y.-Y. 2005, ApJ, 635, L29
Paulino-Afonso, A., Sobral, D., Darvish, B., et al. 2019, A&A, 630, A57
Peng, C. Y., Ho, L. C., Impey, C. D., & Rix, H.-W. 2002, AJ, 124, 266
Peng, Y.-J., Lilly, S. J., Kovač, K., et al. 2010, ApJ, 721, 193
Poggianti, B. M., Desai, V., Finn, R., et al. 2008, ApJ, 684, 888
Salim, S. 2014, Serb. Astron. J., 189, 1
Sánchez, S. F., Avila-Reese, V., Rodríguez-Puebla, A., et al. 2019, MNRAS, 482, 1557

Sazonova, E., Alatalo, K., Lotz, J., et al. 2020, ApJ, 899, 85
Schawinski, K., Urry, C. M., Simmons, B. D., et al. 2014, MNRAS, 440, 889
Schiminovich, D., Wyder, T. K., Martin, D. C., et al. 2007, ApJS, 173, 315
Schmidt, M. 1968, ApJ, 151, 393
Scodeggio, M., Guzzo, L., Garilli, B., et al. 2018, A&A, 609, A84
Scoville, N., Arnouts, S., Aussel, H., et al. 2013, ApJS, 206, 3
Sérsic, J. L. 1963, Boletin de la Asociacion Argentina de Astronomia La Plata Argentina, 6, 41
Siudek, M., Małek, K., Scodeggio, M., et al. 2017, A&A, 597, A107
Siudek, M., Małek, K., Pollo, A., et al. 2018a, A&A, 617, A70
Siudek, M., Małek, K., Pollo, A., et al. 2018b, MNRAS submitted [arXiv:1805.09905]
Skibba, R. A., Bamford, S. P., Nichol, R. C., et al. 2009, MNRAS, 399, 966
Smethurst, R. J., Masters, K. L., Simmons, B. D., et al. 2022, MNRAS, 510, 4126
Socolovsky, M., Almaini, O., Hatch, N. A., et al. 2018, MNRAS, 476, 1242
Socolovsky, M., Maltby, D. T., Hatch, N. A., et al. 2019, MNRAS, 482, 1640
Strateva, I., Ivezić, Ž., Knapp, G. R., et al. 2001, AJ, 122, 1861
Tasca, L. A. M., Kneib, J. P., Iovino, A., et al. 2009, A&A, 503, 379
Thomas, D., Maraston, C., Schawinski, K., Sarzi, M., & Silk, J. 2010, MNRAS, 404, 1775
Toomre, A., & Toomre, J. 1972, ApJ, 178, 623
van Zee, L. 2001, AJ, 121, 2003
Vega-Ferrero, J., Domínguez Sánchez, H., Bernardi, M., et al. 2021, MNRAS, 506, 1927
Vulcani, B., Poggianti, B. M., Finn, R. A., et al. 2010, ApJ, 710, L1
White, S. D. M., & Rees, M. J. 1978, MNRAS, 183, 341

Appendix A: The δ distribution

In Fig. A.1 we show the distribution of $\log(1 + \delta)$ for each VIPERS sub-class.

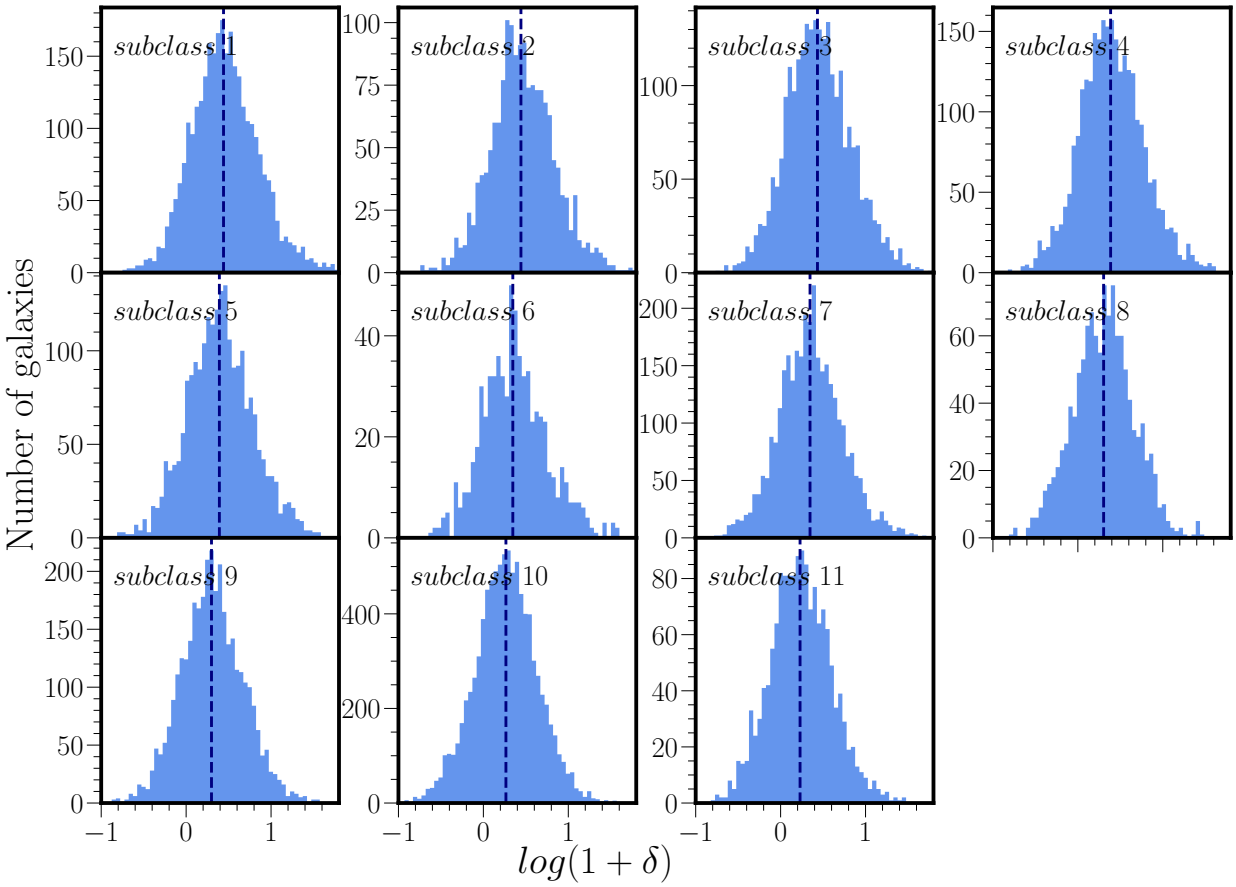

Fig. A.1. Distribution of overdensities for each VIPERS sub-class.